A Novel Endothelial L-Selectin Ligand Activity in Lymph Node Medulla That Is Regulated by α(1,3)-Fucosyltransferase-IV

Christine M'Rini,[1] Guiying Cheng,[1] Colleen Schweitzer,[1] Lois L. Cavanagh,[1,2] Roger T. Palframan,[1,2] Thorsten R. Mempel,[1] Richard A. Warnock,[1,3] John B. Lowe,[4] Elizabeth J. Quackenbush,[1,5] and Ulrich H. von Andrian[1,2]

[1]*CBR Institute for Biomedical Research and* [2]*Department of Pathology, Harvard Medical School, Boston, MA 02115*
[3]*Laboratory of Immunology and Vascular Biology, Department of Pathology, Stanford University Medical School, Stanford, CA 94305*
[4]*Howard Hughes Medical Institute and Department of Pathology, University of Michigan Medical School, Ann Arbor, MI 48109*
[5]*Merck Research Laboratories, Division of Pharmacology, Merck and Company, Rahway, NJ 07065*

Abstract

Lymphocytes home to peripheral lymph nodes (PLNs) via high endothelial venules (HEVs) in the subcortex and incrementally larger collecting venules in the medulla. HEVs express ligands for L-selectin, which mediates lymphocyte rolling. L-selectin counterreceptors in HEVs are recognized by mAb MECA-79, a surrogate marker for molecularly heterogeneous glycans termed peripheral node addressin. By contrast, we find that medullary venules express L-selectin ligands not recognized by MECA-79. Both L-selectin ligands must be fucosylated by α(1,3)-fucosyltransferase (FucT)-IV or FucT-VII as rolling is absent in FucT-IV+VII$^{-/-}$ mice. Intravital microscopy experiments revealed that MECA-79–reactive ligands depend primarily on FucT-VII, whereas MECA-79–independent medullary L-selectin ligands are regulated by FucT-IV. Expression levels of both enzymes paralleled these anatomical distinctions. The relative mRNA level of FucT-IV was higher in medullary venules than in HEVs, whereas FucT-VII was most prominent in HEVs and weak in medullary venules. Thus, two distinct L-selectin ligands are segmentally confined to contiguous microvascular domains in PLNs. Although MECA-79–reactive species predominate in HEVs, medullary venules express another ligand that is spatially, antigenically, and biosynthetically unique. Physiologic relevance for this novel activity in medullary microvessels is suggested by the finding that L-selectin–dependent T cell homing to PLNs was partly insensitive to MECA-79 inhibition.

Key words: homing • intravital microscopy • leukocyte adhesion • leukocyte rolling • vascular addressin

Introduction

Endothelial cells (ECs) in postcapillary and small collecting venules support adhesion and diapedesis of circulating leukocytes, whereas capillaries or arterioles in most organs are essentially nonadhesive. Venules in most lymphoid and some nonlymphoid organs constitutively express adhesion molecules, so-called vascular addressins, and chemokines normally not found in other vascular beds (1). Because vascular addressins are tissue specific, i.e., they are either by themselves or in combination unique to the specialized venular ECs in a particular organ, they regulate the magnitude and composition of leukocyte populations that enter that organ (1, 2). Although some molecular pathways for organ-specific homing of circulating leukocytes are well understood, the cellular and molecular mechanisms that induce and sustain endothelial specialization and vascular addressin expression are still largely unknown.

The online version of this article contains supplemental material.

Address correspondence to Ulrich H. von Andrian, CBR Institute for Biomedical Research and Department of Pathology, Harvard Medical School, 200 Longwood Avenue, Boston, MA 02115. Phone: (617) 278-3130; Fax: (617) 278-3190; email: uva@cbr.med.harvard.edu

Abbreviations used in this paper: BCECF, 2′ 7′,-bis-(2-carboxyethyl)-5 (and 6) carboxyfluorescein; EC, endothelial cell; FucT, α(1,3)-fucosyltransferase; HEV, high endothelial venule; IVM, intravital microscopy; LOV, low order venule; NR, Nile red; PLN, peripheral LN; PNAd, peripheral node addressin; sLeX, sialyl-Lewis^x; TRITC, tetramethylrhodamine-5-isothiocyanate; YG, yellow green.

 J. Exp. Med. © The Rockefeller University Press • 0022-1007/2003/11/1301/12 $8.00
Volume 198, Number 9, November 3, 2003 1301–1312
http://www.jem.org/cgi/doi/10.1084/jem.20030182

The best understood example of endothelium-controlled subset-specific leukocyte recruitment is the homing of lymphocytes to peripheral LNs (PLNs; 3–5). PLNs are strategically positioned to collect antigen via afferent lymphatics, which drain lymph from the periphery into the subcapsular sinus (1, 6). Professional antigen-presenting cells migrate via lymphatics from peripheral tissues into PLNs to interact with lymphocytes. B cells are concentrated within follicles in the PLN cortex, whereas T cells reside in the subcortex and paracortex. Most lymphocytes that home to PLNs and fail to encounter their cognate antigen leave the node by migrating through the medulla into efferent lymph vessels (7).

Blood vessels in different anatomic regions of PLNs possess distinct properties. Typical murine PLNs are supplied by a small artery that penetrates the capsule near the hilus and emits arteriolar branches toward the cortex (8). Arterioles give rise to capillary networks, which merge in the T cell area into high endothelial venules (HEVs) ranging in diameter from ~15–50 μm. HEVs merge into collecting venules lined by flat endothelium in the medulla (9). From here, blood is channeled through hilar vessels into an extranodal vein. The entire venular tree can be visualized by intravital microscopy (IVM) of murine subiliac LNs (superficial inguinal) (8). This structure consists of up to five branching orders where the low order venules (LOVs) comprise a large collecting venule in the hilus (order I) and upstream branches in the medulla (order II and some order III). High order branches are HEVs constituting most order III and all order IV and V venules (8).

Lymphocyte homing occurs mainly in high order HEVs (3, 4). The first step is the binding of L-selectin (CD62L) to endothelial sulfated carbohydrate (CHO) ligands. L-selectin–mediated adhesion is characterized by high on-rate and tensile strength, allowing free-flowing lymphocytes to tether in the presence of shear. Tethered cells roll slowly downstream until they are stimulated by the chemokines CCL21 or CXCL12, which activate LFA-1 integrins whose engagement allows for firm arrest and diapedesis (3–5).

L-selectin is critical for lymphocyte homing to PLNs (10, 11). L-selectin ligands in HEVs are a heterogeneous set of glycan-based structures termed peripheral node addressin (PNAd), which are recognized by mAb MECA-79 (12, 13). The MECA-79 antigen is a core 1–linked, 6-sulfated, sialyl-Lewis^x (sLeX)-like, O-glycan that decorates several endothelial sialomucins, including CD34, GlyCAM-1, podocalyxin, and spg200 (14–17). For L-selectin ligand function, PNAd must be sialylated, sulfated, and α(1,3)-fucosylated (18–22). Thus, PNAd is the result of HEV-specific posttranslational events involving several glycosyltransferases and at least one sulfotransferase.

Required enzymes for PNAd function in vivo are α(1,3)-fucosyltransferase (FucT)-IV, FucT-VII, and the sulfotransferase HEC-GlcNAc6ST (also called LSST or GST-3; 20–22). α(1,3)-fucosylation is particularly essential because homing is abolished in mice that lack both FucT-IV and FucT-VII (22). Although FucT-VII is important for selectin ligand generation (21), homing in FucT-VII$^{-/-}$ mice is less affected than in FucT-IV+VII$^{-/-}$ mice, indicating that FucT-IV compensates partially for FucT-VII deficiency (22). Treatment of mice with mAb MECA-79 inhibits lymphocyte homing to PLNs (12). However, homing is only moderately reduced (~50%) in HEC-GLCNAC6ST$^{-/-}$ mice despite the lack of luminal MECA-79 reactivity in HEVs (20). Thus, MECA-79–reactive PNAd may not be the only endothelial structure recognized by L-selectin in PLN venules.

Here, we provide evidence that LOVs in mouse subiliac LNs express functional L-selectin ligand(s) that are spatially and antigenically distinguishable from MECA-79–reactive PNAd. The MECA-79–reactive material is restricted to paracortical and subcortical venules (order III–V), whereas L-selectin ligand(s) in medullary LOVs are MECA-79$^-$. Moreover, the medullary L-selectin ligand activity is regulated largely by FucT-IV, which is more highly expressed in LOVs than elsewhere in PLNs.

Materials and Methods

Antibodies and Reagents. Antibodies to murine L-selectin (Mel-14), PNAd (MECA-79), sialyl-Lewis$^{X/A}$ (HECA-452), ICAM-2 (mIc2/3c4; provided by T.A. Springer, CBR Institute for Biomedical Research), and human L-selectin (DREG-200) were purified according to standard procedures. FITC-conjugated anti–mouse or rat IgM and IgG (Zymed Laboratories) were used for flow cytometry. Tetramethylrhodamine-5-isothiocyanate (TRITC), 2′ 7′,-bis-(2-carboxyethyl)-5 (and 6) carboxyfluorescein (BCECF), rhodamine 6G, and fluorescent polystyrene microbeads were purchased from Molecular Probes. FITC-dextran was from Sigma-Aldrich.

L1-2 Cell Preparation and Labeling. Murine L1-2 pre–B lymphoma cells transfected with human L-selectin (L1-2$^{L\text{-}selectin}$; reference 13) were grown in RPMI 1640 containing 10% FCS (cRPMI), 250 μg/ml mycophenolic acid, 12.5 μg/ml xanthine, and 1X hypoxanthine/thymidine (GIBCO BRL). For experiments, transfectants that expressed between 70,000 and 100,000 L-selectin molecules/cell were labeled with 2.5 μg/ml BCECF for 30 min.

Flow Cytometry. To assess surface expression of L-selectin on L1-2$^{L\text{-}selectin}$ transfectants, cells were labeled with 20 μg/ml mAb DREG-200 followed by FITC-conjugated anti–mouse IgG, and analyzed using a FACScan™ flow cytometer (BD Biosciences). L-selectin expression was quantified as previously described (23).

Animals. Young adult FucT-deficient mice and WT littermates (C57B1/6 × 129SV) were used (21, 22). T-GFP transgenic mice were generated in our laboratory (24). Mice were kept in a viral antibody-free, specific pathogen-free barrier facility. Experimental procedures were approved by Animal Committees of both Harvard Medical School and The Center for Blood Research in accordance with National Institutes of Health (NIH) guidelines.

Surgical Preparation of Subiliac LN. Mice were anesthetized by intraperitoneal injection of 1 mg/ml xylazine and 5 mg/ml ketamine. The left subiliac LN was prepared for IVM as previously described, and the right femoral artery was catheterized for retrograde injection of fluorescent dyes, cells, beads, or mAbs (8). The preparation was transferred to a customized intravital video microscopy setup (Mikron Instruments) equipped with water immersion objectives (Carl Zeiss MicroImaging, Inc.). Fluorescent

events in the LN microcirculation were visualized by video-triggered stroboscopic epi-illumination (Chadwick Helmuth), recorded by a silicon-intensified target camera (VE1000SIT; Dage MTI), and stored on Hi8 video tape.

Assessment of Intravascular Cell Behavior. Endogenous leukocyte interactions with vascular endothelium were visualized by injection of 1 mg/ml rhodamine 6G (3). In some experiments, 100 μg mAb Mel-14 or MECA-79 (10 mg/kg body weight) were injected i.v., and leukocyte behavior was recorded 15 min thereafter. To visualize L1-2$^{L\text{-selectin}}$ transfectants, BCECF-labeled cells were injected as previously described (8). Luminal surface area of PLN microvessels was calculated from the diameter and length of individual vascular segments (assuming cylindrical geometry) after injection of 150 kD FITC-dextran.

Cell behavior in PLN venules was assessed as previously described (3, 4, 8). The rolling fraction was determined as the percentage of cells that rolled along the vascular lining in the total flux of cells per venule. Rolling cells that arrested for at least 30 s were considered firmly adherent, and their number per luminal surface area was calculated for each venule. Velocity analysis was performed by frame by frame analysis of two representative vessels per experiment as previously described (8). Trajectories of individual cells were traced during passage through capillaries and venules, and their displacement from the point where they first entered the field of view was measured for every video frame. The instantaneous velocity of rolling cells, i.e., the displacement between subsequent video frames (1/30 s), was measured over up to 160 video frames and plotted as a function of time.

In Vivo Mapping of Antigen Densities in PLN Venular Trees. Distribution of MECA-79$^+$ and MECA-79$^-$ venules in PLNs was assessed by injecting CFSE-MECA-79 (1 mg/kg body weight), which leads to specific accumulation of fluorescent mAb in HEV within 10–15 min (25). For semiquantitative assessment of endothelial surface antigen density and distribution in PLN microvessels, protein A–coated yellow green (YG; Ex/Em: 505/515 nm) and Nile red (NR; Ex/Em: 535/575 nm) fluorescent microspheres (1 μm diameter) were labeled with 80 μg/ml anti–rat IgG or IgM. YG beads were incubated with 80 μg/ml MECA-79, HECA-452, or anti–ICAM-2. NR beads were incubated with isotype-matched control mAb. Binding of NR beads in PLN microvessels was recorded 15 min after i.v. injection. After NR beads had disappeared from the circulation (within 30 min), an equivalent amount of YG beads was injected and binding was recorded in the same vessels.

Control experiments performed with control mAb-coated beads revealed no preferential accumulation in particular venular branching orders. To account for random and somewhat variable background binding, bound control NR beads and Ag-specific YG beads were enumerated throughout the entire PLN venular tree (NR_{PLN} and YG_{PLN}, respectively). For the specific accumulation of YG beads, YG_{sp} was determined as $YG_{sp} = YG_{PLN} - NR_{PLN}$, and the specific binding constant (c) was $c = YG_{sp}/YG_{PLN} \times 100$ (%). From the density of adherent YG beads per luminal surface area in each individual venular segment, YG_{ven}, the specific venular concentration, $[YG_{ven}]$, was calculated as: $[YG_{ven}] = YG_{ven} \times c$ (mm^{-2}). The specific arteriolar concentration $[YG_{art}]$ was calculated accordingly.

Homing Experiments. Lymphocyte homing was studied using donor cells from T-GFP mice in which PLN-tropic (i.e., naive and central memory) T cells express GFP, whereas other leukocytes are GFP$^-$ (24, 26). 2×10^7 T-GFP PLN cells were injected i.v. into recipient mice. After 2 h, mice were killed and single cell suspensions were prepared from pooled bilateral subiliac, axillary, and brachial PLNs. The frequency of homed GFP$^+$ T cells was determined by flow cytometry as previously described (4). In some experiments, donor cells were labeled with 30 μg/ml TRITC and homed B cells (GFP$^-$ TRITC$^+$) and T cells (GFP$^+$ TRITC$^+$) were enumerated. To assess the role of MECA-79–reactive and MECA-79–nonreactive L-selectin ligands, three mice received i.v. injections of either 100 μg mAb Mel-14, 10 mg/kg mAb MECA-79, or sterile saline. 15 min later, animals received 2×10^7 T-GFP cells and PLNs were harvested 2 or 24 h thereafter. The number of homed GFP$^+$ cells per 10^6 injected cells was determined for each recipient. Homing in mAb-treated mice was expressed relative to the control mouse that received the same donor cells.

Sorting of PLN ECs. PLNs (inguinal, axillary, brachial, cervical, and popliteal) were collected from 60 young adult C57Bl/6 mice. Single cell suspensions prepared after type II collagenase treatment (Worthington Biochemical Corp.) were depleted of leukocytes using anti-CD45 paramagnetic microbeads (MACS; Miltenyi Biotec). Unbound cells were washed and stained using anti–CD45-CyChrome, anti–MECA79-PE, anti–P-selectin–Ig (BD Biosciences) followed by anti–human Fc-FITC (Caltag), and anti–CD31-biotin (BD Biosciences) followed by streptavidin-ECD (Coulter Immunotech). CD45$^-$ CD31$^+$ ECs from LOVs (MECA-79$^-$ P-selectin-Ig$^+$), HEVs (MECA-79$^+$ P-selectin-Ig$^+$), and nonvenular ECs (MECA-79$^-$ P-selectin-Ig$^-$) were sorted using an EPICS Elite ESP cell sorter (Coulter Corp.).

Analysis of FucT Expression by RT-PCR. EC mRNA was isolated from sorted LOVs (7,630 cells), HEVs (11,500 cells), and nonvenular vessels (20,200 cells) using an RNeasy Mini Kit (QIAGEN). After digesting genomic DNA, cDNA was generated using oligo dT/dNTP mixture (PerkinElmer) with or without Superscript II Reverse Transcriptase (GIBCO BRL). cDNA corresponding to ~1,000 cells/sample was used in each PCR reaction (Hot Star TAq kit; QIAGEN).

Two pairs of primers were added for simultaneous amplification of cDNA pairs for FucT-IV, FucT-VII, and β-actin. Primer sequences (5′-3′) were as follows: FucT-IV sense: TGGACGCGTGGCGAGCCGCGGTGGCCACTCGTGGA, FucT-IV antisense: AACACGCGTAGTACCAGCGCCTTATCCGTGCGTTC; FucT-VII sense: CCTCTCTCTGGGCCCACATCCCCACTACCG, FucT-VII antisense: TCATAGACCTGGCTGCGGGGCAAGTAAGGG; and β-actin sense: TTGGGTATGGAATCCTGTGGCATCCATGAAAC, β-actin antisense: TAAAACGCAGCTCAGTAACAGTCCGCCTAGAA.

PCR amplification was performed on five replicates/sample: step 1, 95°C for 15 min; step 2, 94°C for 1 min; step 3, 70°C for 1 min; step 4, 72°C for 1 min. Steps 2–4 were repeated 39 times. At the end of cycles 31, 33, 35, and 37, one replicate tube from each sample was incubated for 10 min at 72°C. Samples were run on a 4% acrylamide gel in TBE buffer containing ethidium bromide. Empirical analysis of digital images of amplified bands using Adobe Photoshop 6.01 software revealed that samples that underwent 37 amplification cycles yielded optimal results for comparison of relative band intensities. Band intensities were determined as the median channel number in intensity histograms in fixed size regions set over each band. The background fluorescence was determined for each lane and subtracted from specific band signals in the same lane. Relative signal intensity ratios were calculated by dividing the median intensity channel of the larger amplicon by that of the smaller one.

Statistics. For statistical comparison of two samples, a two-tailed Student's *t* test was used. Multiple comparisons were performed using the Kruskal-Wallis test with Bonferroni correction.

Differences were considered statistically significant when $P < 0.05$. Data are presented as mean ± SEM.

Online Supplemental Material. Video 1 illustrates the topography of MECA-79–reactive L-selectin ligands in a mouse PLN. Videos 2–4 document the behavior of L1-2 cells in a PLN. Video 5 shows an animated three-dimensional reconstruction of serial confocal sections through a subiliac LN 24 h after treatment with mAb MECA-79 and adoptive transfer of green fluorescent T cells. Fig. S1 is a schematic diagram of the microvascular anatomy shown in Videos 2–4. Videos 1–5 and Fig. S1 are available at http://www.jem.org/cgi/content/full/jem.20030182/DC1.

Results and Discussion

L-Selectin Ligands Are Expressed in Both MECA-79$^+$ HEVs and MECA-79$^-$ LOVs. Previous IVM observations of murine subiliac LNs illustrate a striking distinction between different segments of the venular tree with regard to reactivity with CFSE-labeled anti-PNAd mAb MECA-79 (25). After i.v. injection of fluorescent mAb, paracortical and subcortical postcapillary and small collecting venules (orders III–V) were brightly stained, whereas most large collecting LOVs in the medulla (orders I–II) were not (Fig. 1 A). Because MECA-79–reactive glycans are considered the critical L-selectin ligands in PLNs, LOVs should support little or no L-selectin–mediated rolling. However, primary mouse lymphocytes and stably transfected L1-2$^{L\text{-selectin}}$ cells rolled in order I and II venules, albeit at a lower frequency than in high order venules (3, 8, 25, 27).

We examined this apparent discrepancy between segmentally confined MECA-79 reactivity, and broad venular L-selectin ligand activity using L1-2$^{L\text{-selectin}}$ transfectants. CFSE-labeled MECA-79 was injected at a dose (20 μg/mouse) sufficient to label MECA-79$^+$ microvessels, but less

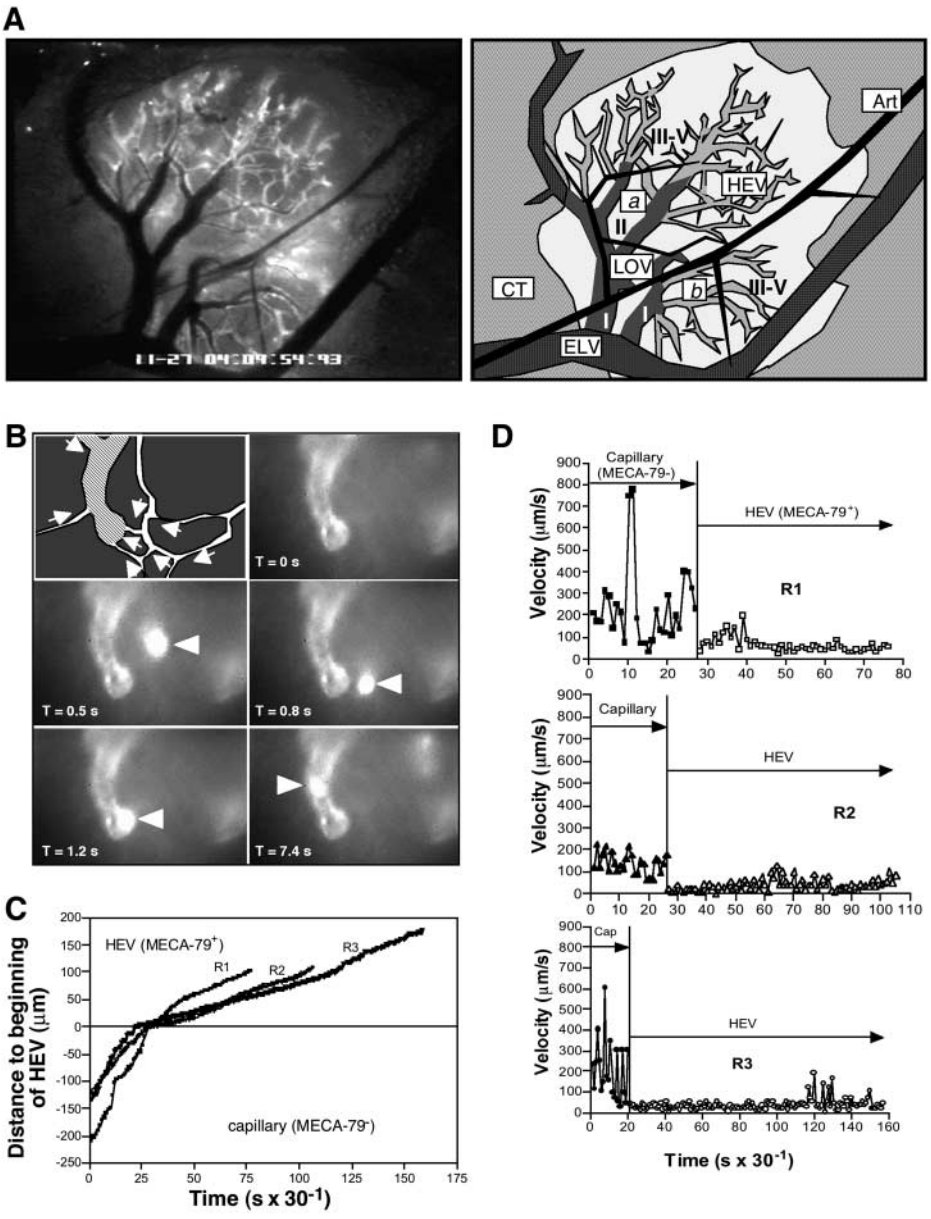

Figure 1. EC adhesiveness and expression of MECA-79 epitope changes abruptly on transition from capillaries to HEVs. (A) CFSE-MECA-79 staining of two venular trees (*a* and *b*) in a subiliac PLN (left), with major anatomic features illustrated schematically (right). Blood enters PLN capillaries (not visible) via branches of the superficial epigastric artery (Art). Postcapillary and small collecting HEVs (orders III–V, light gray) are MECA-79$^+$, but low order medullary venules (LOV, orders I–II, dark gray) and extra-lymphoid veins (ELV) are not. The PLN is surrounded by connective tissue (CT). ×40. (B) PLN subcortex showing capillary network (arrows indicate direction of blood flow) draining into an order V HEV (hatched). CFSE-MECA-79 delineates the sharp transition from capillaries to HEV (T = 0 s). A fluorescent lymphocyte (arrowhead) passes through a capillary at high velocity (T = 0.5 – 0.8 s), tethers to MECA-79$^+$ ECs (T = 1.2 s), and rolls slowly along the HEV (T = 7.4 s). The capillary network was subsequently visualized by injecting FITC-dextran (not depicted). ×400. (C) Displacement histograms of three L1-2$^{L\text{-selectin}}$ cells (R1, R2, and R3) during transition from capillaries into HEVs. A cell enters the field of view at time 0. The distance of the cell to the transition from MECA-79$^-$ ECs to MECA-79$^+$ HEVs was determined for every video frame until the cell disappeared from the field of view. (D) Instantaneous velocity histograms of L1-2$^{L\text{-selectin}}$ cells, R1–R3, shown in C during their passage through capillaries and HEVs. See also Video 1, available at http://www.jem.org/cgi/content/full/jem.20030182/DC1.

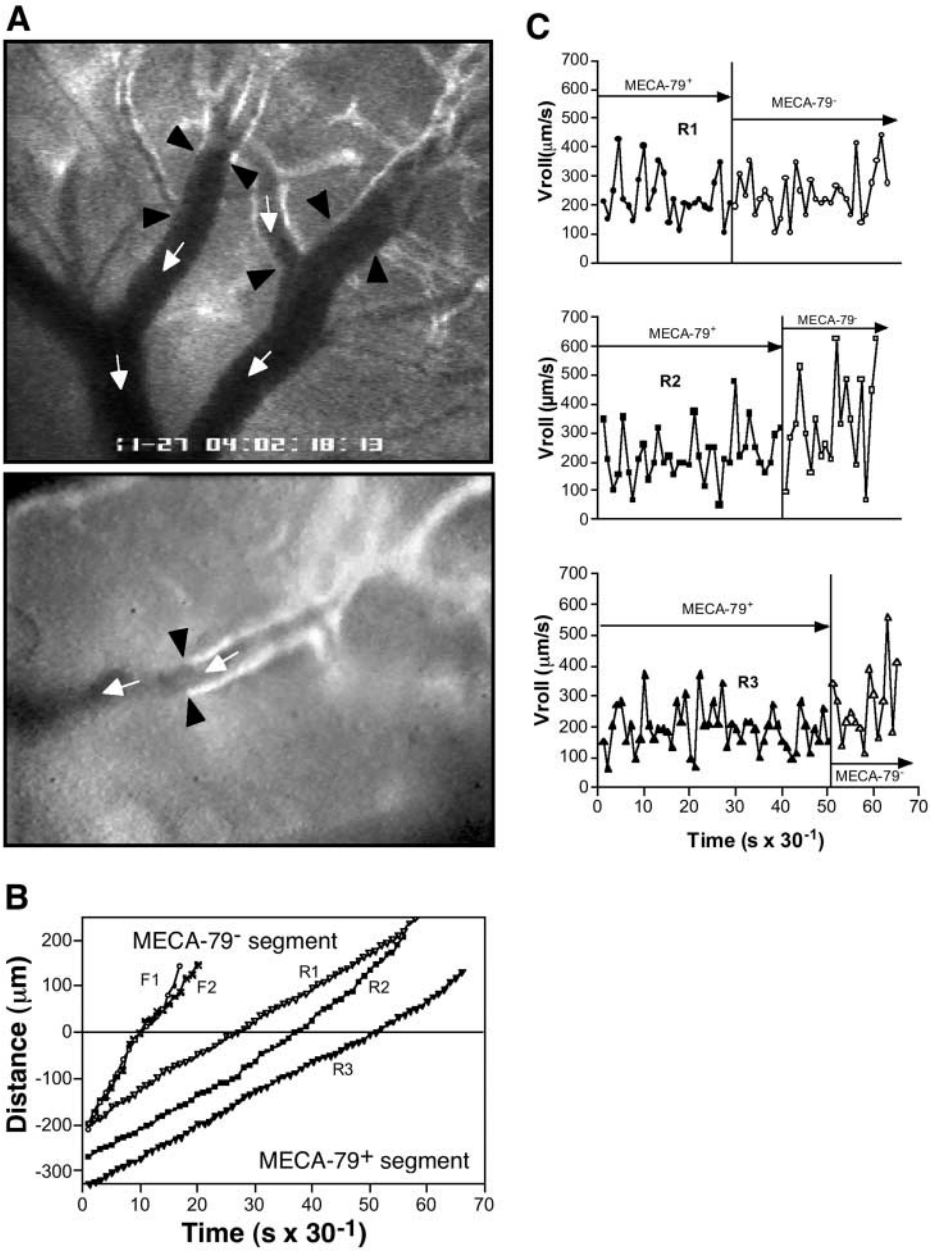

Figure 2. L-selectin transfectants roll throughout the PLN venular tree despite discontinuous expression of MECA-79 epitopes. (A) Micrographs illustrating the abrupt transition from MECA-79$^+$ to MECA-79$^-$ ECs in PLN venules in a segment of venular tree *a* in Fig. 1 A (top panel; ×100), and an order III venule from a different preparation (bottom panel; ×200). Transition from MECA-79$^-$ to MECA-79$^+$ ECs (black arrowheads) often coincided with venular bifurcations (top panel), but was also seen within continuous venular segments (bottom panel). White arrows indicate direction of blood flow. (B) Displacement histograms of two noninteracting fast cells (F1 and F2) and three rolling cells (R1–R3) in MECA-79$^+$ and MECA-79$^-$ segments of the same venule. Cells were analyzed as in Fig. 1 C. (C) Instantaneous velocity histograms of the three rolling cells, R1–R3, shown in panel B.

than necessary for inhibition of L-selectin binding in high order venules (see below). Consistent with previous studies (8, 27), many L1-2$^{L\text{-selectin}}$ cells rolled in high order venules immediately after entry from capillaries (Fig. 1, B–D), whereas control transfectants did not.

MECA-79 staining ended abruptly in LOVs, seemingly between adjacent ECs. Loss of immunoreactivity often coincided with vessel bifurcations, but occasionally staining disappeared midway along an order II or III venule, unrelated to any other apparent anatomic features (Fig. 2 A). The rolling fraction of L1-2$^{L\text{-selectin}}$ cells was highest in order IV and V venules, decreasing further downstream as the rolling cells detached and rejoined the fast moving blood stream (8, 27). However, detachment occurred throughout the venular tree and did not coincide with the disappearance of MECA-79 staining. Indeed, L1-2$^{L\text{-selectin}}$ cells continued rolling as they passed from MECA-79$^+$ to MECA-79$^-$ LOVs, without appreciable immediate changes in velocity (Fig. 2 B). L-selectin–mediated rolling is relatively jerky (28), which was somewhat more apparent in MECA-79$^-$ than MECA-79$^+$ venules (Fig. 2 C). However, as is typical for microvascular leukocyte behavior, there was considerable heterogeneity even within MECA-79$^+$ venular segments because the immediate postcapillary venules supported smoother and slower rolling than most downstream venules.

Segmental Differences in Adhesion Molecule Expression between Different Branching Orders in PLN Venules. The rolling behavior of L1-2$^{L\text{-selectin}}$ cells together with the CFSE-MECA-79 staining pattern suggested the existence of

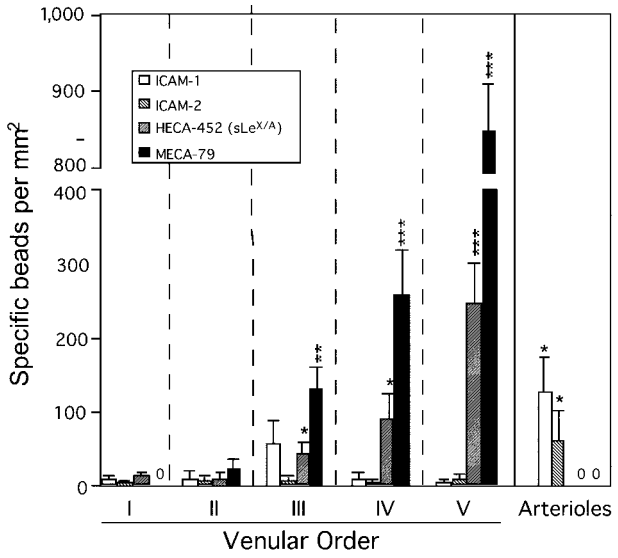

Figure 3. Fluorescent bead accumulation in PLNs reveals segmental differences in luminal antigen expression between venular branching orders. Binding of nonspecific mAb-coated NR and specific mAb-coated YG fluorescent beads in PLN microvessels 15 min after i.v. injection. NR beads were injected first, followed by an equivalent number of YG beads coated with mAb MECA-79, anti-$sLe^{X/A}$ (HECA-452), anti–ICAM-1, or anti–ICAM-2. The accumulation of specific beads was calculated as described in Materials and Methods. All specific mAb-coated beads bound significantly more than control beads, except for MECA-79–coated beads in order I venules, and both MECA-79 and anti-$sLe^{X/A}$–coated beads in arterioles. *, $P < 0.05$; **, $P < 0.01$; ***, $P < 0.001$ compared with order I venules. Number of LNs/venules analyzed: 9/54 for ICAM-1; 3/46 for ICAM-2; 5/77 for $sLe^{X/A}$; and 4/45 for MECA-79.

MECA-79–insensitive L-selectin ligand(s) in LOVs. To eliminate the possibility of a low density MECA-79–reactive ligand that was undetectable using video microscopy, we established a more sensitive, semiquantitative assay to analyze luminal surface antigens in PLNs. Polystyrene beads (1 μm diameter) emitting either YG or NR fluorescence were coated with mAbs against endothelial adhesion molecules or control mAbs, respectively. Equivalent numbers of beads were successively injected into mice and branching order-specific bead accumulation was determined in PLNs (Fig. 3).

MECA-79–coated beads mirrored fluorescent mAb labeling, as there was a dramatic accumulation of beads in high order venules, whereas bead binding was very sparse in order II and undetectable in order I venules. Anti-$sLe^{X/A}$–coated beads were similarly distributed, with some additional binding in order I. Neither set of beads bound to arterioles or arteries, whereas beads coated with anti–ICAM-1 or anti–ICAM-2 adhered to these microvessels. Anti-ICAM beads also bound to PLN venules, but at relatively low density and without preference for any particular branching order. Nevertheless, anti–ICAM-1– and anti–ICAM-2–coated beads accumulated 2.7- and 2.1-fold more than control beads, a ratio that was in the same range as seen with beads to P-selectin or VCAM-1 in bone marrow microvessels (29).

It should be cautioned that differences in bead accumulation between mAbs may not necessarily reflect different absolute densities of endothelial antigens. Factors including the number of functional binding sites per bead, mAb affinity, avidity, and accessibility of cognate epitopes are important. For example, MECA-79 and HECA-452 are multivalent IgMs recognizing CHO-capping groups in the endothelial glycocalyx, whereas anti–ICAM-1 and anti–ICAM-2 are bivalent IgGs that bind epitopes on the core of glycoproteins located close to the cell membrane. Nevertheless, this assay provides a relative measure of the intravascular accessibility and relative abundance of endothelial surface molecules in the microcirculation.

Because anti-ICAM–coated beads showed no statistically significant preference for any particular venular order, the skewedness in MECA-79– and anti-$sLe^{X/A}$ –coated bead distribution toward high order venules cannot be explained by segmentally distinct microhemodynamics. Rather, the findings indicate that MECA-79–reactive glycans are only expressed in high order venules and are absent from LOVs. $sLe^{X/A}$ has a similar distribution, but is expressed at a low level in order I venules.

MECA-79 Blocks L-Selectin Tethering Only in High Order PLN Venules. Because LOVs are devoid of MECA-79 reactivity, but support L-selectin binding, we postulated that MECA-79 treatment should not affect rolling in LOVs. Saturating amounts of MECA-79 (10 mg/kg) nearly abolished rolling of $L1\text{-}2^{L\text{-selectin}}$ cells in high order venules, but reduced rolling in LOVs only slightly (Fig. 4 A). This partial inhibition by MECA-79 in LOVs was not necessarily caused by locally expressed MECA-79 antigen because most cells that rolled in LOVs initially tethered in upstream $MECA\text{-}79^{+}$ segments (Fig. 2, B and C). If margination in high order venules is prevented by MECA-79, fewer cells are likely to interact downstream even if LOVs express different L-selectin ligand(s). Indeed, MECA-79 had no significant effect when only those $L1\text{-}2^{L\text{-selectin}}$ cells that were free flowing in high order venules and initiated rolling after entering LOVs were taken into account (Fig. 4 B).

These findings indicate that MECA-79–reactive L-selectin ligands are restricted to high order venules, whereas L-selectin binding to LOVs is mediated by a second, antigenically distinct L-selectin ligand. The nearly complete inhibition of rolling by MECA-79 in high order venules suggests that the two L-selectin ligands have distinct spatial expression patterns with little overlap along the venular tree.

MECA-79–independent L-Selectin Ligands Mediate T Cell Homing to PLNs. We tested the relative contribution of MECA-79–reactive and nonreactive L-selectin ligands to lymphocyte homing in PLNs. We used T-GFP mice in which PLN-tropic naive and central memory T cell subsets express GFP (4, 26, 30). Consistent with recent findings (31), treatment with MECA-79 abrogated T cell accumulation in WT PLNs at 2 h (Fig. 4 C). However, short-term homing may not be sufficiently sensitive to detect subtle contributions by other ligands. Indeed, after 24 h, PLNs in MECA-79–treated recipients contained 83.7 ± 4.5%

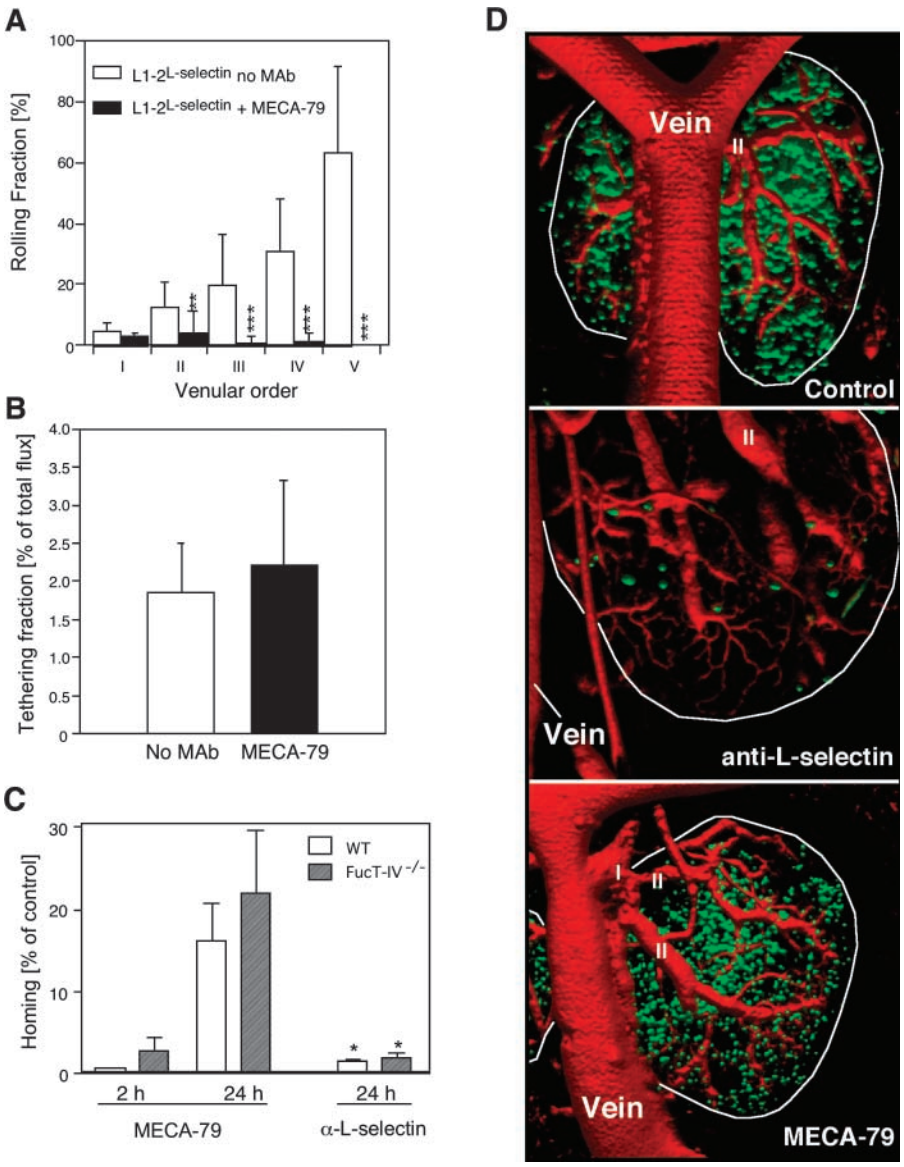

Figure 4. Effect of MECA-79 on L-selectin–dependent lymphocyte homing and rolling in PLNs. (A) The rolling fraction of L1-2$^{L\text{-selectin}}$ cells was analyzed before and after MECA-79 treatment (10 mg/kg i.v.) in each branching order of PLN venular trees (n = 6 mice). mAb treatment blocked rolling in order II–V venules (**, $P < 0.01$; ***, $P < 0.001$ vs. no mAb), but had minimal effect in order I venules. (B) Tethering fraction of L1-2$^{L\text{-selectin}}$ cells in order I and II venules before and after PNAd inhibition. Only free-flowing cells that established the first adhesive contact with LOVs were counted. See also Videos 2–4, available at http://www.jem.org/cgi/content/full/jem.20030182/DC1. (C) L-selectin–mediated homing of naive T cells to PLNs is partially insensitive to MECA-79 inhibition. MECA-79 treatment (10 mg/kg, 15 min before T cell injection) abrogated T cell homing to PLNs harvested 2 h after cell injection (n = 2). 24 h of treatment with MECA-79 (15 min before and 12 h after T cell injection) reduced homing significantly less than anti–L-selectin mAb Mel-14 (100 μg/mouse). Results were normalized to untreated control mice. n = 4 mice/group; *, $P < 0.05$ versus 24 h MECA-79. (D) 3-D reconstruction of serial confocal micrographs showing homed T cells (green) in inguinal LNs 24 h after treatment with saline (top), anti–L-selectin mAb Mel-14 (middle), or MECA-79 (bottom). The intravascular compartment was delineated by i.v. injection of TRITC-dextran (red). Numerous extravascular T cells are dispersed throughout control and MECA-79–treated PLNs, including in the vicinity of LOVs (order I and II venules). A nearby extralymphoid vein drains blood from the node. LN borders are demarcated by white lines. See also Video 5, available at http://www.jem.org/cgi/content/full/jem.20030182/DC1.

(mean ± SEM) fewer homed cells than in control mice, compared with 98.6 ± 0.2% inhibition with anti–L-selectin ($P < 0.05$; n = 4 mice/group).

Serum MECA-79 decreased from 30 μg/ml at 2 h to 5 μg/ml at 24 h after a single injection. To increase the mAb concentration at 24 h, two mice received an additional injection of 10 mg/kg MECA-79 12 h after T cell transfer, resulting in 27 μg/ml MECA-79 at 24 h. Despite these different blood levels, T cell homing was equivalent (82 vs. 86% inhibition), indicating that both treatment regimens achieved maximal inhibition of homing.

T cells that homed to PLNs of MECA-79–treated recipients were not trapped in microvessels but resided throughout the T cell area, some in the vicinity of LOVs (Fig. 4 D). Because homed T cells migrate rapidly and in random directions as soon as they have passed across HEVs (32), localization of homed cells may not necessarily reflect the microvascular segment in which they became initially adherent. Nevertheless, these data strongly suggest that a significant fraction of L-selectin–dependent T cell homing to PLNs is insensitive to MECA-79 inhibition.

L-Selectin–mediated Rolling Has Distinct Requirements for FucT-IV and FucT-VII in High Order Venules and LOVs. Although physiologic selectin ligands require α(1,3)-fucosylation by FucT-VII and, to a lesser degree, by FucT-IV, the MECA-79 epitope is not fucosylation dependent (21, 22, 33, 34). Recent work has shown that MECA-79 epitopes are associated with core 1–linked O-glycans whose intravascular expression depends on 6-sulfation of a GlcNAc residue by the HEV-specific sulfotransferase, HEC-GLCNAC6ST (17, 20, 31). Nevertheless, fucosylation is essential for L-selectin ligand function in PLN HEVs because lymphocyte homing is markedly reduced (by ~80%) in PLNs of FucT-VII$^{-/-}$ mice, and the homing defect is significantly more severe in FucT-IV+VII$^{-/-}$ doubly deficient mice (22). To assess the role of fucosylation for

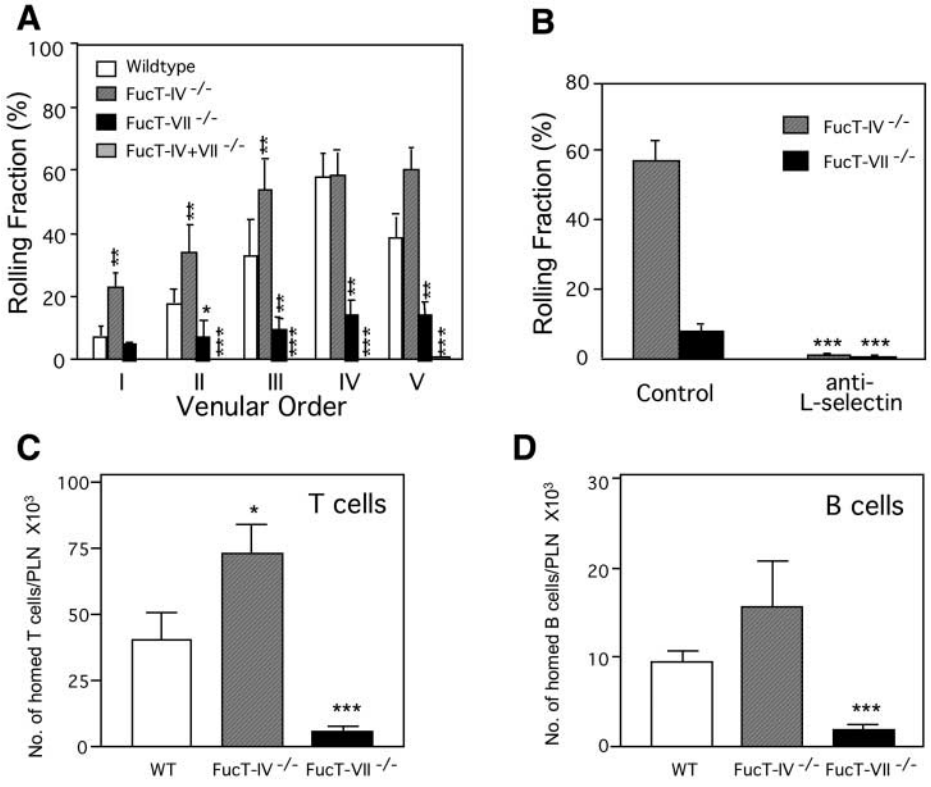

Figure 5. Role of FucT-IV and FucT-VII in lymphocyte homing and L-selectin ligand activity in PLN venules. (A) Rolling fractions of rhodamine 6G-labeled leukocytes were assessed in each venular order of PLN from WT and mutant mice. Rolling was absent in FucT-IV+VII$^{-/-}$ PLNs. Compared with WT mice, rolling in FucT-VII$^{-/-}$ PLNs was markedly lower in order III–V HEVs, modestly decreased in order II, and unchanged in order I venules. Rolling in order I–III venules of FucT-IV$^{-/-}$ PLNs was significantly higher than in WT PLNs, whereas rolling in order IV and V venules was similar. *, $P < 0.05$; **, $P < 0.01$; ***, $P < 0.001$ versus WT. (B) Leukocyte rolling in FucT-IV$^{-/-}$ and FucT-VII$^{-/-}$ PLNs before and after injection of anti–L-selectin (100 μg/mouse). ***, $P < 0.001$ versus control; $n = 3$ mice/group. (C) Compared with WT mice, naive T cell homing was enhanced in FucT-IV$^{-/-}$ mice and severely compromised in FucT-VII$^{-/-}$ mice. *, $P < 0.05$ versus WT; ***, $P < 0.001$ versus WT and FucT-IV$^{-/-}$; $n = 4$ mice/group. (D) B cell homing required FucT-VII and was somewhat increased in FucT-IV$^{-/-}$ PLNs ($P > 0.05$). ***, $P < 0.001$ versus WT and FucT-IV$^{-/-}$; $n = 4$ mice/group.

L-selectin ligand(s) in LOVs, we compared the rolling behavior of rhodamine 6G-labeled circulating leukocytes in each venular order in PLNs of WT and FucT-deficient mice.

As expected, rolling was completely absent in FucT-IV+VII$^{-/-}$ PLNs, indicating that all L-selectin ligands are obligatorily α(1,3)-fucosylation dependent (Fig. 5 A). However, the relative importance of FucT-IV and FucT-VII depended on anatomic localization. In high order venules rolling was predominantly dependent on FucT-VII. Some residual rolling was observed in HEVs of FucT-VII$^{-/-}$ mice, but not in doubly deficient PLNs, indicating a minor role of FucT-IV. This FucT-IV–dependent ligand activity was blocked by MECA-79 treatment (Fig. 4 A and unpublished data). However, because MECA-79 is an IgM of relatively high molecular weight (12) and accumulates to high density in HEVs, we cannot exclude that FucT-IV generates L-selectin ligand(s) that are structurally distinct from the MECA-79 antigen, but still inhibitable by MECA-79 possibly due to steric hindrance.

Unexpectedly, rolling in LOVs was similar in WT and FucT-VII$^{-/-}$ PLNs and significantly increased in FucT-IV$^{-/-}$ PLNs. Anti–L-selectin mAb Mel-14 abrogated rolling in all venules of both FucT-IV$^{-/-}$ and FucT-VII$^{-/-}$ PLNs, indicating that deletion of FucT genes did not induce compensatory up-regulation of other rolling pathways (Fig. 5 B). Anti–L-selectin inhibited leukocyte rolling in mutant mice even more completely than in WT animals where P-selectin mediates some L-selectin–independent rolling (35). This is expected because FucT-IV and FucT-VII contribute to P-selectin ligand generation (22, 36). Enhanced rolling observed in LOVs of FucT-IV$^{-/-}$ PLNs was due to the absence of FucT-IV in ECs, not leukocytes, as lymphocytes from WT and FucT-IV$^{-/-}$ donors rolled equivalently in FucT-IV$^{-/-}$ PLNs (unpublished data).

Together, these findings imply segmentally distinct enzyme requirements for venular L-selectin ligand generation. Although FucT-VII predominates in high order venules where the MECA-79 epitope is strongly expressed, FucT-IV prevails in LOVs because rolling was minimally affected in medullary venules of FucT-VII$^{-/-}$ PLNs. However, FucT-VII can also generate L-selectin ligands in LOVs because rolling was significantly enhanced in FucT-IV$^{-/-}$ LOVs, but completely lost in FucT-IV+VII$^{-/-}$ PLNs.

Naive T Cell Homing Is Enhanced in PLNs of FucT-IV$^{-/-}$ Mice. Because FucT-IV deficiency unexpectedly boosted L-selectin–dependent rolling in LOVs, we sought to determine the physiologic significance of this observation for lymphocyte homing. Earlier studies using a mixture of naive and memory B and T cells from mesenteric LNs found a trend toward increased homing in FucT-IV$^{-/-}$ PLNs, but this was not statistically significant (22). Because different lymphocyte populations have distinct PLN tropism (30, 37), the inherent variability in homing of mixed lymphocyte populations might obscure subset-specific effects in FucT-IV$^{-/-}$ PLNs. Therefore, we stained T-GFP lymphocytes with the red fluorophore TRITC for subset-specific homing studies in PLNs of WT, FucT-IV$^{-/-}$, or FucT-VII$^{-/-}$ recipients.

As predicted by our IVM studies and consistent with previous reports (21, 22), both GFP$^+$ TRITC$^+$ T cells (Fig. 5 C) and GFP$^-$ TRITC$^+$ B cells (Fig. 5 D) homed poorly to FucT-VII$^{-/-}$ PLNs ($P < 0.001$). Strikingly, FucT-IV$^{-/-}$ PLNs contained ~87% more donor T cells than WT PLNs ($P < 0.05$). Average B cell homing was also 67% higher in FucT-IV$^{-/-}$ PLNs, but this was quite variable ($P > 0.05$). Thus, FucT-IV exerts an attenuating effect on T cell homing to PLNs, presumably by reducing availability of L-selectin ligands in LOVs. On the other hand, homing is more severely compromised in FucT-IV+VII$^{-/-}$ PLNs than in FucT-VII$^{-/-}$ PLNs (22), indicating an additional adhesion-promoting role for FucT-IV–dependent glycans, at least in FucT-VII$^{-/-}$ mice, which was also confirmed by our IVM studies. Given the prominent role of FucT-IV in L-selectin ligand production in LOVs, it seems likely that MECA-79–insensitive L-selectin ligands in these vessels can contribute to the physiologic entry of lymphocytes into WT PLNs. Accordingly, we observed L-selectin–dependent, MECA-79–insensitive T cell homing to PLNs in FucT-IV$^{-/-}$ mice, which was somewhat more pronounced than in WT mice (Fig. 4 C).

Selectin Ligand Activity in LOVs Is Transcriptionally Determined by the Balance of FucT-IV and FucT-VII Expression. To explain why FucT-IV deficiency increases FucT-VII–dependent L-selectin ligand activity in LOVs, one must consider the acceptor preferences of FucT-IV and FucT-VII (38, 39). FucT-VII requires α(2,3)-sialylated terminal lactosamine to generate sLe^X-like selectin ligands. FucT-IV can also use the sialylated lactosamine substrate, albeit less efficiently than FucT-VII. However, unlike FucT-VII, FucT-IV additionally fucosylates internal GlcNAc residues in polylactosamine (38) and uses nonsialylated lactosamine to generate Lewis^X-like structures (22), which do not interact with selectins. Thus, FucT-IV may compete with α(2,3)sialyltransferase(s) and/or FucT-VII for terminal lactosamine as a shared precursor substrate on O-linked glycans. Consequently, FucT-IV may divert some terminal lactosamine acceptor moieties toward the Lewis^x pathway that does not yield L-selectin ligands, and thus away from the α(2,3)sialyltransferase/FucT-VII synthetic route. In LOVs of WT mice, FucT-IV could thus attenuate FucT-VII–dependent production of sLe^X-based L-selectin ligands. Without FucT-IV, increased acceptor availability for α(2,3)sialyltransferase/FucT-VII permits increased selectin ligand production, whereas FucT-VII deficiency might have lesser impact because sLe^X-based L-selectin ligands could still be generated if FucT-IV is abundantly expressed.

Given these considerations, we hypothesized that venular L-selectin ligands in PLNs are regulated, in part, by the balance of FucT-IV and FucT-VII expression. FucT-VII is transcriptionally regulated by diverse external factors. It is induced postnatally in developing murine PLN HEVs. In adult PLNs, FucT-VII expression is transiently down-regulated upon antigenic challenge, and afferent lymph flow is essential for steady-state expression (40). Whether endothelial FucT-IV is also subjected to spatial and/or temporal regulation has not been examined.

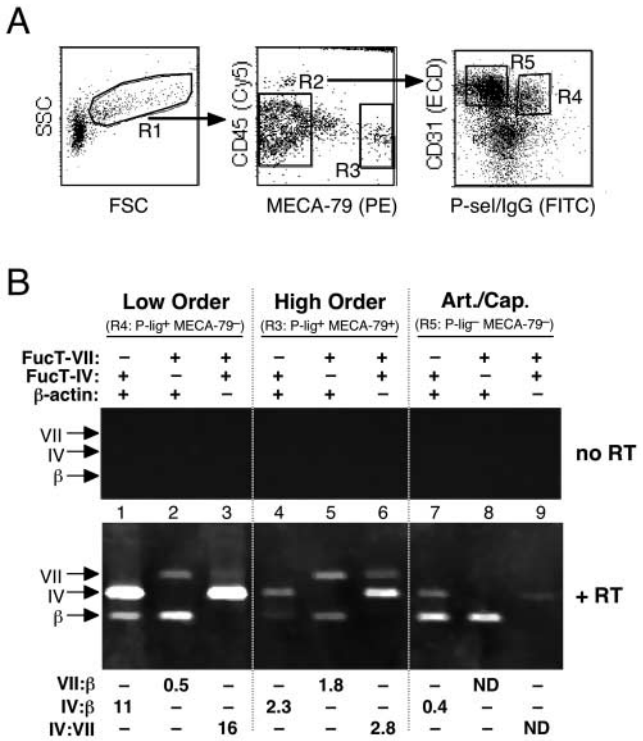

Figure 6. Differential expression of FucT-IV and FucT-VII in PLN ECs. (A) Leukocyte-depleted cell suspensions from PLNs of 60 WT mice were stained for the pan-leukocyte antigen CD45, MECA-79, pan-endothelial CD31, and P-selectin–Ig chimera ligands. After gating on large cells (R1), ECs from high order venules were identified as CD45$^-$ MECA-79$^+$ (R3) as well as CD31$^+$ and P-selectin–Ig binding (P-lig$^+$; not depicted). ECs from other vascular segments were isolated from the CD45$^-$ MECA-79$^-$ fraction (R2) by gating on CD31$^+$ cells. P-lig$^+$ ECs were from LOVs (R4), and nonvenular ECs (MECA-79$^-$ P-lig$^-$) were from capillaries, arterioles, and possibly lymph vessels (R5). (B) mRNA from equivalent numbers of sorted ECs from LOVs (lanes 1–3), high order venules (lanes 4–6), and nonvenular vessels (lanes 7–9) was subjected to RT-PCR with and without addition of reverse transcriptase (RT) followed by competitive PCR amplification (37 cycles) of pairs of cDNAs for FucT-IV, FucT-VII, and the housekeeping gene β-actin. The intensity ratios of amplified bands in each lane are shown. Intensity ratios could not be determined (ND) in lanes 8 and 9 because no specific signal for FucT-VII transcripts was detectable in nonvenular ECs. The PCR procedure was repeated twice with similar results.

Based on a combination of EC-specific antigenicity (CD45$^-$ CD31$^+$) and differential selectin ligand expression, we sorted three distinct EC populations from PLNs (Fig. 6 A): (a) nonvenular MECA-79$^-$ ECs (from capillaries, some arterioles, and possibly lymphatics) that did not express selectin ligands, (b) MECA-79$^+$ ECs from high order venules, and (c) MECA-79$^-$ ECs from LOVs expressing selectin ligands. To identify the latter, we exploited the fact that PLN venules support not only binding of L-selectin, but also P-selectin and E-selectin (27, 41). Indeed, both P-selectin$^+$ activated platelets and L1-2$^{P\text{-selectin}}$ transfectants tethered and rolled efficiently in LOVs, but not in capillaries or arterioles (unpublished data). Thus, LOV ECs were defined as MECA-79$^-$ CD45$^-$ CD31$^+$ cells that bound P-selectin–Ig chimeric protein. Substituting P-selectin–Ig for L-selectin–Ig facilitated this approach, because L-selec-

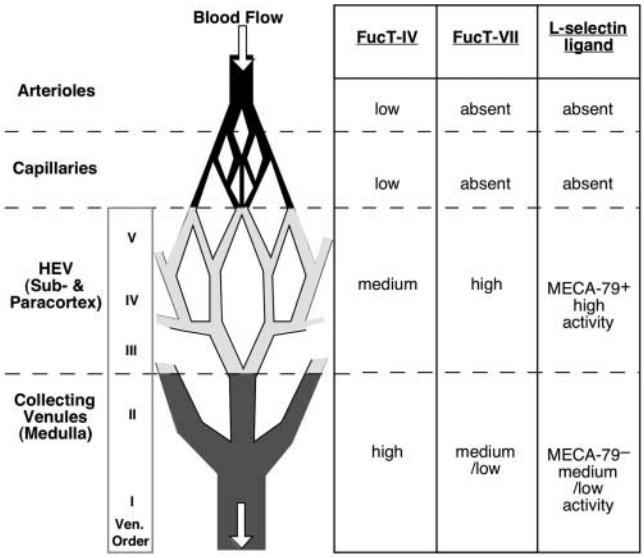

Figure 7. Distribution of functional L-selectin ligands and of FucT-IV and FucT-VII in PLN microvessels.

tin–Ig yielded poor staining (unpublished data), presumably due to the shorter bond lifetime and/or the more pronounced requirement for fluid shear that distinguish L-selectin from P-selectin bonds (28, 42, 43).

EC subsets were sorted from PLNs pooled from 60 donor mice, which yielded a total of 11,500 ECs from HEVs, 7,500 LOV ECs, and 20,200 nonvenular ECs. Subsequently, sorted cells were lysed and subjected to multiplex RT-PCR. Each PCR reaction contained cDNA from equivalent numbers of cells, and two pairs of primers for simultaneous amplification of FucT-IV, FucT-VII, and/or β-actin. Digital images of amplicon bands were measured by densitometry. Although this approach did not allow direct quantitation of absolute mRNA levels, signal intensity ratios for each pair of amplicons could be reasonably determined. Thus, we generated a side by side comparison of FucT-IV and FucT-VII expression relative to each other and to β-actin in each EC population (Fig. 6 B).

The results of this semiquantitative analysis, which was repeated twice with similar results, were in excellent agreement with our hypothesis. FucT-IV was present in all EC samples, but relative to β-actin its expression in nonvenular endothelium was ~27 and ~6 times lower than in LOVs and high order venules, respectively. In contrast, FucT-VII was only detectable in venular ECs and, compared with β-actin, FucT-VII mRNA was 3.6 times more abundant in high order venules than in LOVs. Strikingly, the FucT-IV/FucT-VII ratio was 5.7 times higher in LOVs than in HEVs.

Topography and Biochemistry of L-Selectin Ligands in PLNs. Assuming that β-actin expression is invariable in PLN ECs, a map of the relative expression levels of FucT-IV and FucT-VII can be generated (Fig. 7). FucT-IV predominates in LOVs where it may generate primarily nonsialylated fucosylated glycans, limiting production to one (or possibly more) sialylated L-selectin ligand(s) that is (are) antigenically distinct from the MECA-79 epitope. Although the precise structure of this molecule remains to be solved, the absence of rolling in FucT-IV+VII$^{-/-}$ mice shows a clear requirement for α(1,3) fucosylation. In the absence of FucT-IV, activity of this ligand is enhanced possibly due to increased substrate availability for FucT-VII. However, FucT-IV probably dominates the physiologic ligand generation because FucT-VII deficiency had minimal impact on LOV adhesiveness.

Whether the medullary L-selectin ligand requires sulfation for normal activity is unclear. In animals deficient in HEC-GlcNAc6ST, an HEV-expressed sulfotransferase required for luminal expression of MECA-79 epitopes, L-selectin–dependent lymphocyte homing to PLNs is reduced by ~50%, and lymphocytes roll in all venules at normal frequency, but with accelerated velocity (20, 31). This confirms that HEC-GlcNAc6ST–dependent sulfation (and luminal MECA-79 expression) is important, but not essential for L-selectin ligand expression in PLNs. We demonstrate that MECA-79–independent L-selectin ligands are not merely a peculiarity of HEC-GlcNAc6ST$^{-/-}$ PLNs, but they also facilitate T cell rolling and homing in WT PLNs. MECA-79–insensitive L-selectin binding was also observed in human tonsils (44). This activity was resistant to digestion with O-sialoglycoprotease, which destroys sialomucins that present MECA-79 epitopes. Conceivably, medullary L-selectin ligands may not only differ from MECA-79–reactive ligands in their antigenicity and topography, but also in the scaffold on which they are presented.

The sialomucin CD43 antagonizes L-selectin–dependent T cell tethering and rolling in PLNs (25). This antiadhesive effect is greater in LOVs than high order HEVs. This suggests that the ultrastructure and/or microenvironment of medullary L-selectin ligands differ from those in high order venules, thus allowing large, anionic surface molecules such as CD43 to exert increased antiadhesive activity in LOVs. Interestingly, FucT-VII modifies only glycoproteins, whereas FucT-IV also generates sLe^X-containing glycolipids that support L-selectin binding in vitro (45, 46). Because rolling on glycolipids requires a closer proximity of surface membranes, it might be more sensitive to interference by CD43. However, whether FucT-IV–dependent glycolipids can support in vivo L-selectin binding in LOVs or elsewhere remains to be determined.

Venular ECs in many nonlymphoid vascular beds express L-selectin ligands when exposed to inflammation (47, 48), including heparin-like molecules, which do not require fucosylation for functional activity (49). Moreover, expression of nonlymphoid endothelial L-selectin ligands is delayed (about 1 h) in response to inflammatory stimuli (50). Conversely, we observed rolling of endogenous leukocytes, isolated lymphocytes, and L1-2$^{L\text{-selectin}}$ cells in LOVs immediately after surgical preparation of PLNs (~20 min after the initial skin incision), which was constant over several hours (unpublished data). Thus, although it cannot be excluded that the medullary L-selectin ligand(s) described here share(s) biochemical properties with L-selectin ligands elsewhere, its spatial restriction and constitutive expression in LOVs strongly suggest that this activity is unique to PLN medulla.

Although the medulla is arguably the least understood region in PLNs, its cellular composition is distinct from cortical regions. The medulla contains columns of macrophages, plasma cells, and T cells of mostly memory phenotype. It is assumed that these cells migrate to the medulla from other regions through the PLN parenchyma. Alternatively, some of these relatively rare leukocytes might be recruited via medullary venules, which we show here to constitute a specialized microvascular environment expressing at least one unique leukocyte traffic molecule. However, L-selectin alone would not be sufficient for leukocyte homing to the medulla because L-selectin allows cells only to roll, but not arrest. For this, an integrin-activating chemoattractant and endothelial integrin ligands are necessary. For example, in PLN HEVs, integrin activation on rolling T and B cells is mediated by CCL21 and CXCL12 (4, 5). Monocytes also home to PLNs that drain inflamed tissues via CCL2 transported to PLNs via afferent lymph vessels, and presented in HEVs to stimulate integrin-mediated monocyte arrest (51). Interestingly, our previous IVM observations using fluorescent mAbs to CCL21 or fluorescent CCL2 indicate that these chemokines are not tightly restricted to HEVs, but are present in medullary venules (unpublished data). Moreover, significant segmental differences were not revealed in expression of ICAM-1 and ICAM-2 within the venular tree (Fig. 3). Thus, all prerequisite components of multistep adhesion cascades are present in medullary venules. However, the magnitude, composition, and physiologic significance of cellular traffic through these microvessels must be further examined.

We thank Eugene Butcher for providing mAbs, and Natalia Souchkova and Bruce Reinhardt for expert technical assistance.

This study was supported by NIH grants HL48675, HL54936, and HL56949 to U.H. von Andrian. C. M'Rini, R.T. Palframan, and E.J. Quackenbush were supported by stipends from NATO, the Wellcome Trust, and a Pfizer Scholars Grant from Children's Hospital, respectively.

Submitted: 3 February 2003
Revised: 18 August 2003
Accepted: 24 September 2003

References

1. von Andrian, U.H., and C.R. Mackay. 2000. T-cell function and migration. Two sides of the same coin. *N. Engl. J. Med.* 343:1020–1034.
2. Springer, T.A. 1994. Traffic signals for lymphocyte recirculation and leukocyte emigration: the multi-step paradigm. *Cell.* 76:301–314.
3. Warnock, R.A., S. Askari, E.C. Butcher, and U.H. von Andrian. 1998. Molecular mechanisms of lymphocyte homing to peripheral lymph nodes. *J. Exp. Med.* 187:205–216.
4. Stein, J.V., A. Rot, Y. Luo, M. Narasimhaswamy, H. Nakano, M.D. Gunn, A. Matsuzawa, E.J. Quackenbush, M.E. Dorf, and U.H. von Andrian. 2000. The CC chemokine thymus-derived chemotactic agent 4 (TCA-4, secondary lymphoid tissue chemokine, 6Ckine, exodus-2) triggers lymphocyte function–associated antigen 1–mediated arrest of rolling T lymphocytes in peripheral lymph node high endothelial venules. *J. Exp. Med.* 191:61–76.
5. Okada, T., V.N. Ngo, E.H. Ekland, R. Forster, M. Lipp, D.R. Littman, and J.G. Cyster. 2002. Chemokine requirements for B cell entry to lymph nodes and Peyer's patches. *J. Exp. Med.* 196:65–75.
6. Gretz, J.E., A.O. Anderson, and S. Shaw. 1997. Cords, channels, corridors and conduits: critical artichitectural elements facilitating cell interactions in the lymph node cortex. *Immunol. Rev.* 156:11–24.
7. Gowans, J.L., and E.J. Knight. 1964. The route of re-circulation of lymphocytes in the rat. *Proc. R. Soc. Lond. B. Biol. Sci.* 159:257–282.
8. von Andrian, U.H. 1996. Intravital microscopy of the peripheral lymph node microcirculation in mice. *Microcirculation.* 3:287–300.
9. De Bruyn, P.P., and Y. Cho. 1990. Structure and function of high endothelial postcapillary venules in lymphocyte circulation. *Nature.* 84:85–101.
10. Gallatin, W.M., I.L. Weissman, and E.C. Butcher. 1983. A cell-surface molecule involved in organ-specific homing of lymphocytes. *Nature.* 304:30–34.
11. Arbones, M.L., D.C. Ord, K. Ley, H. Ratech, C. Maynard-Curry, G. Otten, D.J. Capon, and T.F. Tedder. 1994. Lymphocyte homing and leukocyte rolling and migration are impaired in L-selectin-deficient mice. *Immunity.* 1:247–260.
12. Streeter, P.R., B.T.N. Rouse, and E.C. Butcher. 1988. Immunohistologic and functional characterization of a vascular addressin involved in lymphocyte homing into peripheral lymph nodes. *J. Cell Biol.* 107:1853–1862.
13. Berg, E.L., M.K. Robinson, R.A. Warnock, and E.C. Butcher. 1991. The human peripheral lymph node vascular addressin is a ligand for LECAM-1, the peripheral lymph node homing receptor. *J. Cell Biol.* 114:343–349.
14. Lasky, L.A., M.S. Singer, D. Dowbenko, Y. Imai, W.J. Henzel, C. Grimley, C. Fennie, N. Gillett, S.R. Watson, and S.D. Rosen. 1992. An endothelial ligand for L-selectin is a novel mucin-like molecule. *Cell.* 69:927–938.
15. Baumhueter, S., M.S. Singer, W. Henzel, S. Hemmerich, M. Renz, S.D. Rosen, and L.A. Lasky. 1993. Binding of L-selectin to the vascular sialomucin, CD34. *Science.* 262:436–438.
16. Sassetti, C., K. Tangemann, M.S. Singer, D.B. Kershaw, and S.D. Rosen. 1998. Identification of podocalyxin-like protein as a high endothelial venule ligand for L-selectin: parallels to CD34. *J. Exp. Med.* 187:1965–1975.
17. Yeh, J.C., N. Hiraoka, B. Petryniak, J. Nakayama, L.G. Ellies, D. Rabuka, O. Hindsgaul, J.D. Marth, J.B. Lowe, and M. Fukuda. 2001. Novel sulfated lymphocyte homing receptors and their control by a Core1 extension beta 1,3-N-acetylglucosaminyltransferase. *Cell.* 105:957–969.
18. Rosen, S.D., S.I. Chi, D.D. True, M.S. Singer, and T.A. Yednock. 1989. Intraveneously injected sialidase inactivates attachment sites for lymphocytes on high endothelial venules. *J. Immunol.* 142:1895–1902.
19. Hemmerich, S., E.C. Butcher, and S.D. Rosen. 1994. Sulfation-dependent recognition of high endothelial venules (HEV)-ligands by L-selectin and MECA 79. *J. Exp. Med.* 180:2219–2226.
20. Hemmerich, S., A. Bistrup, M.S. Singer, A. van Zante, J.K. Lee, D. Tsay, M. Peters, J.L. Carminati, T.J. Brennan, K. Carver-Moore, et al. 2001. Sulfation of L-selectin ligands by an HEV-restricted sulfotransferase regulates lymphocyte homing to lymph nodes. *Immunity.* 15:237–247.

21. Maly, P., A.D. Thall, B. Petryniak, C.E. Rogers, P.L. Smith, R.M. Marks, R.J. Kelly, K.M. Gersten, G. Cheng, T.L. Saunders, et al. 1996. The α(1,3) fucosyltransferase Fuc-TVII controls leukocyte trafficking through an essential role in L-, E-, and P-selectin ligand biosynthesis. *Cell*. 86:643–653.
22. Homeister, J.W., A.D. Thall, B. Petryniak, P. Maly, C.E. Rogers, P.L. Smith, R.J. Kelly, K.M. Gersten, S.W. Askari, G. Cheng, et al. 2001. The alpha(1,3)fucosyltransferases FucT-IV and FucT-VII exert collaborative control over selectin-dependent leukocyte recruitment and lymphocyte homing. *Immunity*. 15:115–126.
23. von Andrian, U.H., S.R. Hasslen, R.D. Nelson, S.L. Erlandsen, and E.C. Butcher. 1995. A central role for microvillous receptor presentation in leukocyte adhesion under flow. *Cell*. 82:989–999.
24. Manjunath, N., P. Shankar, B. Stockton, P.D. Dubey, J. Lieberman, and U.H. von Andrian. 1999. A transgenic mouse model to analyze CD8(+) effector T cell differentiation in vivo. *Proc. Natl. Acad. Sci. USA*. 96:13932–13937.
25. Stockton, B.M., G. Cheng, N. Manjunath, B. Ardman, and U.H. von Andrian. 1998. Negative regulation of T cell homing by CD43. *Immunity*. 8:373–381.
26. Manjunath, N., P. Shankar, J. Wan, W. Weninger, M.A. Crowley, K. Hieshima, T.A. Springer, X. Fan, H. Shen, J. Lieberman, et al. 2001. Effector differentiation is not prerequisite for generation of memory cytotoxic T lymphocytes. *J. Clin. Invest*. 108:871–878.
27. Stein, J.V., G. Cheng, B.M. Stockton, B.P. Fors, E.C. Butcher, and U.H. von Andrian. 1999. L-selectin–mediated leukocyte adhesion in vivo: microvillous distribution determines tethering efficiency, but not rolling velocity. *J. Exp. Med*. 189:37–50.
28. Alon, R., S. Chen, K.D. Puri, E.B. Finger, and T.A. Springer. 1997. The kinetics of L-selectin tethers and the mechanics of selectin-mediated rolling. *J. Cell Biol*. 138:1169–1180.
29. Mazo, I.B., E.J. Quackenbush, J.B. Lowe, and U.H. von Andrian. 2002. Total body irradiation causes profound changes in endothelial traffic molecules for hematopoietic progenitor cell recruitment to bone marrow. *Blood*. 99:4182–4191.
30. Weninger, W., M.A. Crowley, N. Manjunath, and U.H. von Andrian. 2001. Migratory properties of naive, effector, and memory $CD8^+$ T cells. *J. Exp. Med*. 194:953–966.
31. van Zante, A., J.-M. Gauguet, A. Bistrup, D. Tsay, U.H. von Andrian, and S.D. Rosen. Lymphocyte–HEV interactions in lymph nodes of a sulfotransferase-deficient mouse. *J. Exp. Med*. 198:1289–1300.
32. Miller, M.J., S.H. Wei, M.D. Cahalan, and I. Parker. 2003. Autonomous T cell trafficking examined in vivo with intravital two-photon microscopy. *Proc. Natl. Acad. Sci. USA*. 100:2604–2609.
33. Hemmerich, S., and S.D. Rosen. 1994. 6'-Sulfated sialyl Lewis x is a major capping group of GlyCAM-1. *Biochemistry*. 33:4830–4835.
34. Hemmerich, S., H. Leffler, and S.D. Rosen. 1995. Structure of the O-glycans in glyCAM-1, an endothelial-derived ligand for L-selectin. *J. Biol. Chem*. 270:12035–12047.
35. Diacovo, T.G., M.D. Catalina, M.H. Siegelman, and U.H. von Andrian. 1998. Circulating activated platelets reconstitute lymphocyte homing and immunity in L-selectin–deficient mice. *J. Exp. Med*. 187:197–204.
36. Weninger, W., L.H. Ulfman, G. Cheng, N. Souchkova, E.J. Quackenbush, J.B. Lowe, and U.H. von Andrian. 2000. Specialized contributions by alpha(1,3)-fucosyltransferase-IV and FucT-VII during leukocyte rolling in dermal microvessels. *Immunity*. 12:665–676.
37. Tang, M.L., D.A. Steeber, X.Q. Zhang, and T.F. Tedder. 1998. Intrinsic differences in L-selectin expression levels affect T and B lymphocyte subset-specific recirculation pathways. *J. Immunol*. 160:5113–5121.
38. Niemela, R., J. Natunen, M.L. Majuri, H. Maaheimo, J. Helin, J.B. Lowe, O. Renkonen, and R. Renkonen. 1998. Complementory acceptor and site specificities of Fuc-TIV and Fuc-TVII allow effective biosynthesis of sialyl-TriLex and related polylactosamines present on glycoprotein counterreceptors of selectins. *J. Biol. Chem*. 273:4021–4026.
39. Lowe, J.B. 2001. Glycosylation, immunity, and autoimmunity. *Cell*. 104:809–812.
40. Swarte, V.V., D.H. Joziasse, D.H. Van den Eijnden, B. Petryniak, J.B. Lowe, G. Kraal, and R.E. Mebius. 1998. Regulation of fucosyltransferase-VII expression in peripheral lymph node high endothelial venules. *Eur. J. Immunol*. 28:3040–3047.
41. Diacovo, T.G., K.D. Puri, R.A. Warnock, T.A. Springer, and U.H. von Andrian. 1996. Platelet-mediated lymphocyte delivery to high endothelial venules. *Science*. 273:252–255.
42. Finger, E.B., K.D. Puri, R. Alon, M.B. Lawrence, U.H. von Andrian, and T.A. Springer. 1996. Adhesion through L-selectin requires a threshold hydrodynamic shear. *Nature*. 379:266–269.
43. Puri, K.D., E.B. Finger, and T.A. Springer. 1997. The faster kinetics of L-selectin than of E-selectin and P-selectin rolling at comparable binding strength. *J. Immunol*. 158:405–413.
44. Clark, R.A., R.C. Fuhlbrigge, and T.A. Springer. 1998. L-selectin ligands that are O-glycoprotease-resistant and distinct from MECA-79 antigen are sufficient for tethering and rolling of lymphocytes on human high endothelial venules. *J. Cell Biol*. 140:721–731.
45. Huang, M.C., A. Laskowska, D. Vestweber, and M.K. Wild. 2002. The alpha (1,3)-fucosyltransferase Fuc-TIV, but not Fuc-TVII, generates sialyl Lewis X-like epitopes preferentially on glycolipids. *J. Biol. Chem*. 277:47786–47795.
46. Alon, R., T. Feizi, C.-T. Yuen, R.C. Fuhlbrigge, and T.A. Springer. 1995. Glycolipid ligands for selectins support leukocyte tethering and rolling under physiologic flow conditions. *J. Immunol*. 154:5356–5366.
47. von Andrian, U.H., J.D. Chambers, L.M. McEvoy, R.F. Bargatze, K.E. Arfors, and E.C. Butcher. 1991. Two-step model of leukocyte-endothelial cell interaction in inflammation: distinct roles for LECAM-1 and the leukocyte β_2 integrins *in vivo*. *Proc. Natl. Acad. Sci. USA*. 88:7538–7542.
48. Ley, K., P. Gaehtgens, C. Fennie, M.S. Singer, L.A. Lasky, and S.D. Rosen. 1991. Lectin-like cell adhesion molecule 1 mediates leukocyte rolling in mesenteric venules in vivo. *Blood*. 77:2553–2555.
49. Norgard-Sumnicht, K.E., N.M. Varki, and A. Varki. 1993. Calcium-dependent heparin-like ligands for L-selectin in nonlymphoid endothelial cells. *Science*. 261:480–483.
50. Ley, K., D.C. Bullard, M.L. Arbonés, R. Bosse, D. Vestweber, T.F. Tedder, and A.L. Beaudet. 1995. Sequential contribution of L- and P-selectin to leukocyte rolling in vivo. *J. Exp. Med*. 181:669–675.
51. Palframan, R.T., S. Jung, G. Cheng, W. Weninger, Y. Luo, M. Dorf, D.R. Littman, B.J. Rollins, H. Zweerink, A. Rot, et al. 2001. Inflammatory chemokine transport and presentation in HEV: a remote control mechanism for monocyte recruitment to lymph nodes in inflamed tissues. *J. Exp. Med*. 194:1361–1374.